

Ring Vortex/Cylinder Sound Production Revisited

Jay C. Hardin*

NASA Langley Research Center, Hampton, Virginia

and

D. S. Pope†

PRC Kentron, Inc., Hampton, Virginia

The acoustic radiation produced by the passage of a vortex ring near a circular cylinder is calculated using the Coriolis acceleration of the vortex as the source term and the low-frequency Green's function approach. The vortex path is allowed to be arbitrary, and necessary integrals are evaluated exactly via complex integration techniques. The results exhibit good agreement (on a Pascal basis) with experimental data. Of particular interest is the rotation of the directivity pattern during this transient encounter and the extreme sensitivity of the results to the distance at which the vortex passes by the cylinder.

Introduction

THE acoustic radiation produced by the passage of a ring vortex near a circular cylinder has recently been studied, both theoretically and experimentally, by Minota and Kambe.¹ This seemingly academic problem is of interest in several respects. First, it is a fully three-dimensional problem that is analytically tractable. Second, a ring vortex is easily produced in a laboratory; thus, a clean experiment can be performed for precise comparison with the theoretical results. Finally, study of this model problem should help one to understand curvature effects associated with other geometries, such as in helicopter blade/vortex interaction.

The analytical treatment developed by Minota and Kambe¹ was based upon the theory of Obermeier² in which the aeroacoustic source term is shown to depend linearly upon vorticity and the concept of a vector Green's function is employed. Application of this theory to the ring vortex/cylinder problem led to two fundamental integrals upon which the sound radiation depends. Minota and Kambe evaluated these integrals by expanding the integrands in power series in a small parameter ϵ and neglecting higher order terms. However, the agreement between theory and experiment was not as good as one might hope, which Minota and Kambe attributed to the fact that the small parameter ($\epsilon = 0.34$) was larger than might be desired.

In the present paper, this problem is re-analyzed using the theory of Howe,³ in which the aeroacoustic source term depends upon the Coriolis acceleration (vorticity cross velocity) of the flow and the low-frequency Green's function is employed. This analysis expands on that presented by Minota and Kambe¹ in two ways. First, the path of the vortex, which Minota and Kambe had prescribed to be linear, is allowed to be arbitrary. Since, as will be seen in the analysis, the precise position of the vortex with respect to the cylinder is very important to the noise generation process. This freedom in the

analysis allows for the natural deviation of the vortex path due to the presence of the cylinder. Second, the theory leads to precisely the same integrals (although with more variable parameters) upon which the sound field depends as those obtained by Minota and Kambe¹ before the integrands were expanded. In this analysis, these two fundamental integrals are evaluated exactly using complex integration techniques, thus removing the small parameter approximation of Minota and Kambe.¹ The resulting acoustic pressure signatures are then compared with experimental data.

Analysis

Consider the geometry shown in Fig. 1. A ring vortex of strength Γ and radius r_v is moving due to its self-convection velocity in the presence of a circular cylinder of radius b . The coordinate system is placed with its origin at the center of the cylinder and such that the centerline of the vortex is in the plane $y_3 = 0$. Due to the symmetry, the vortex centerline will always remain in this plane. The vortex is assumed to pass far enough away from the cylinder that any distortion of its shape is negligible. Thus, the center of the vortex translates along the path $[Y_1(t), Y_2(t), 0]$. An observer is at the far-field position x , shown on the figure. If the convection Mach number is low, i.e., $M = V_s/a_o \ll 1$, where $V_s = \sqrt{\dot{Y}_1^2 + \dot{Y}_2^2}$ is the vortex speed and a_o is the speed of sound in the medium, the theory

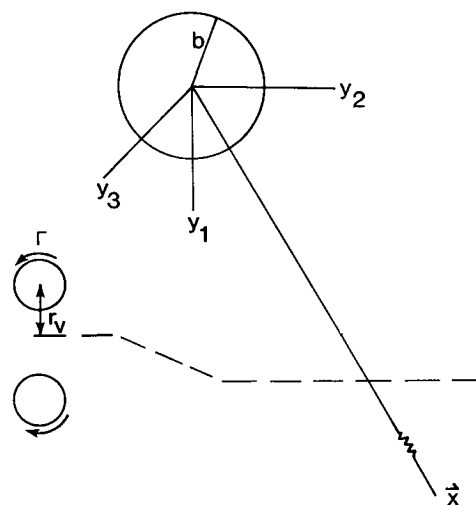


Fig. 1 Geometry of the problem.

Received Aug. 7, 1987; presented as Paper 87-2671 at the AIAA 11th Aeroacoustics Conference, Sunnydale, CA, Oct. 19-21, 1987; revision received Dec. 4, 1987. Copyright © American Institute of Aeronautics and Astronautics, Inc., 1988. No copyright is asserted in the United States under Title 17, U.S. Code. The U.S. Government has a royalty-free license to exercise all rights under the copyright claimed herein for Governmental purposes. All other rights are reserved by the copyright owner.

*Senior Research Scientist, Aeroacoustics Branch.

†Project Engineer.

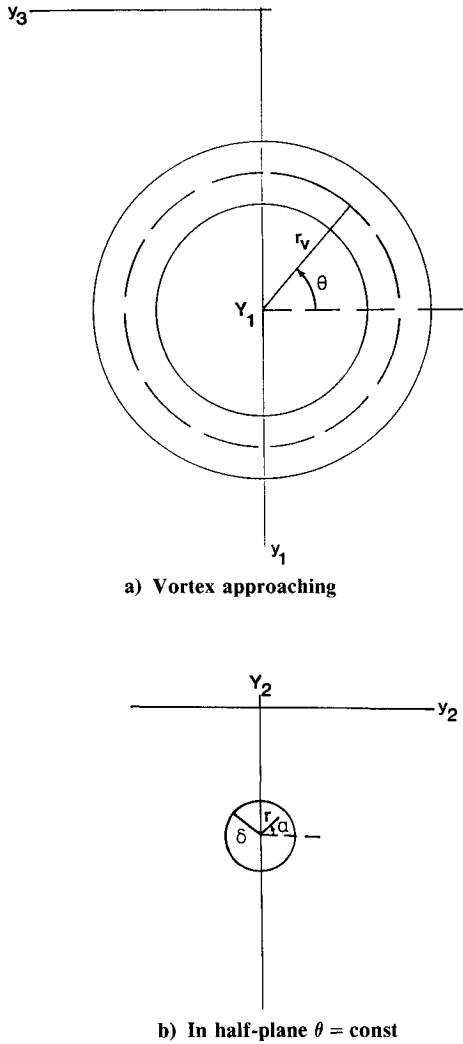


Fig. 2 Toroidal coordinate system.

of Howe³ may be employed to express the acoustic pressure radiated to the far-field observer as

$$p\left(x, t + \frac{x}{a_o}\right) = \frac{-\rho_o}{4\pi a_o x} \frac{\partial}{\partial t} \int_{\text{vol}} (\Omega x v) \cdot \nabla \left(\frac{x}{x} \cdot \phi \right) dy \quad (1)$$

where t is the time, $x = |x|$, ρ_o is the density of the medium, Ω and v are the vorticity and velocity within the flowfield, and

$$\Phi = [y_1(1 + b^2/\rho^2), y_2(1 + b^2/\rho^2), y_3]$$

where

$$\rho^2 = y_1^2 + y_2^2$$

Since the vorticity is nonzero only within the vortex itself, the volume integral reduces to an integral over the vortex. Thus introduce the change of variable

$$y_1 = Y_1 - (r_v + r \sin \alpha) \sin \theta$$

$$y_2 = Y_2 + r \cos \alpha$$

$$y_3 = - (r_v + r \sin \alpha) \cos \theta$$

as shown in Fig. 2, where the magnitude of the Jacobian of the transformation is $r(r_v + r \sin \alpha)$. The vortex core radius is taken as δ . Within this core, the vorticity is assumed to be uniform, such that

$$\Gamma = \pi \delta^2 \Omega \quad (2)$$

Now, note that $\delta/Y_1 \ll 1$. Thus, the integrand of Eq. (1) can be expanded in a power series in (r/Y_1) and higher order terms neglected (since $r < \delta$). This produces

$$\begin{aligned} p\left(x, t + \frac{x}{a_o}\right) &\approx \frac{-\rho_o r_v}{4\pi a_o x} \frac{\partial}{\partial t} \\ &\times \int_0^{2\pi} d\theta \int_0^{2\pi} d\alpha \int_0^\delta dr r \left[(\Omega x v) \cdot \nabla \left(\frac{x}{x} \cdot \Phi \right) \right] \\ &= \frac{-\rho_o r_v \delta^2}{4a_o x} \frac{\partial}{\partial t} \int_0^{2\pi} d\theta \left[(\Omega x v) \cdot \nabla \left(\frac{x}{x} \cdot \Phi \right) \right] \end{aligned} \quad (3)$$

to order $(\delta/Y_1)^3$, where the terms in brackets are evaluated at $r=0$. Further,

$$\Omega = [-\Omega \cos \theta, 0, \Omega \sin \theta]$$

and where $r=0$, $v = [\dot{Y}_1, \dot{Y}_2, 0]$. Thus, using Eq. (2), Eq. (3) becomes

$$\begin{aligned} p\left(x, t + \frac{x}{a_o}\right) &= \frac{\rho_o \Gamma b^2}{4\pi a_o x} \frac{\partial}{\partial t} \left[\frac{\epsilon \dot{Y}_1}{Y_1} \left(\frac{x_2}{x} I_1 \right. \right. \\ &\left. \left. + \frac{2x_1}{x} y_c I_2 \right) + \frac{\epsilon \dot{Y}_2}{Y_1} \left(\frac{x_1}{x} I_1 - \frac{2x_2}{x} y_c I_2 \right) \right] \end{aligned} \quad (4)$$

where

$$y_c(t) = Y_2(t)/Y_1(t)$$

$$\epsilon(t) = r_v/Y_1(t)$$

$$I_1(y_c, \epsilon) = \int_0^{2\pi} \frac{[y_c^2 - (1 - \epsilon \sin \theta)^2] \sin \theta d\theta}{[y_c^2 + (1 - \epsilon \sin \theta)^2]^2}$$

$$I_2(y_c, \epsilon) = \int_0^{2\pi} \frac{(1 - \epsilon \sin \theta) \sin \theta d\theta}{[y_c^2 + (1 - \epsilon \sin \theta)^2]^2}$$

Equation (4), for the case $Y_1(t) = \text{const}$, is precisely the result obtained by Minota and Kambe,¹ using Obermeier's² approach, before expanding the integrands in powers of ϵ .

Now, note that if the complex variable $z = e^{i\theta}$ is introduced, these integrals can be written as contour integrals around the unit circle, i.e.,

$$I(y_2, \epsilon) = \frac{-8}{\epsilon^4} \oint \frac{p_1(z) dz}{f^2(z)} \quad (5)$$

$$I_2(y_c, \epsilon) = \frac{-4i}{\epsilon} \oint \frac{p_2(z) dz}{f^2(z)} \quad (6)$$

where

$$p_1(z) = (z^2 - 1) [2y_c^2 z^2 + \epsilon^2/4f(z)]$$

$$p_2(z) = z(z^2 - 1)(z^2 - 2i/\epsilon z - 1)$$

$$f(z) = (z - z_1)(z - z_2)(z - z_3)(z - z_4)$$

Here, the z_i are the roots

$$z_1 = \frac{1}{\epsilon} [(|y_c| + \sqrt{s_1}) + i(1 + \sqrt{s_2})]$$

$$z_2 = \frac{1}{\epsilon} [(|y_c| - \sqrt{s_1}) + i(1 - \sqrt{s_2})]$$

$$z_3 = \frac{-1}{\epsilon} [(|y_c| - \sqrt{s_1}) - i(1 - \sqrt{s_2})]$$

$$z_4 = \frac{-1}{\epsilon} [(|y_c| + \sqrt{s_1}) - i(1 + \sqrt{s_2})]$$

where

$$s_{1,2} = \frac{1}{2} \sqrt{(\epsilon^2 + y_c^2 - 1)^2 + 4y_c^2} \pm \frac{1}{2} (\epsilon^2 + y_c^2 - 1)$$

Thus, the integrals may be evaluated by summing their residues at poles inside the unit circle.

The imaginary part of the roots z_1 and z_4 is quite large, and thus they never enter the unit circle. However, the roots z_2 and z_3 lie within the unit circle at all times. Figure 3 presents the loci of the roots z_2 and z_3 for $-3 < y_c < 3$ and ϵ fixed as 0.34. Note that since $z_3 = -z_2^*$, both roots traverse the same path in opposite directions, becoming equal and purely imaginary at $y_c = 0$.

The preceding analysis indicates that the integrals given by Eq. (5) and (6) have poles of order two at the points $z = z_2$ and $z = z_3$ inside the unit circle. Summing the residues at these poles yields the expressions

$$I_1(y_c, \epsilon) = \frac{-128\pi y_c^2 i (z_2 + z_3) [(1 - z_2 z_3)^2 - z_2 z_3 (1 + z_2^2)(1 + z_3^2)]}{\epsilon^4 (z_2 - z_1)(z_2 - z_4)(z_3 - z_1)(z_3 - z_4)(1 + z_2^2)(1 + z_3^2)(1 + z_2 z_3)} - \frac{8\pi i}{\epsilon^2} \frac{[(z_2 + z_3) - (z_1 + z_4)]}{(z_2 - z_1)(z_2 - z_4)(z_3 - z_1)(z_3 - z_4)}$$

$$I_2(y_c, \epsilon) = \frac{16\pi}{\epsilon^3} \frac{(1 - z_2 z_3) [(z_2^2 + z_3^2)(1 + z_2 z_3 + z_2^2 z_3^2) + z_2 z_3 (1 + 4z_2 z_3 + z_2^2 z_3^2)]}{(1 + z_1 z_4)(1 + z_2^2)^3 (1 + z_3^2)^3}$$

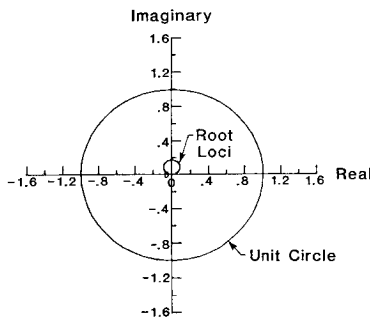


Fig. 3 Loci of roots z_2 and z_3 .

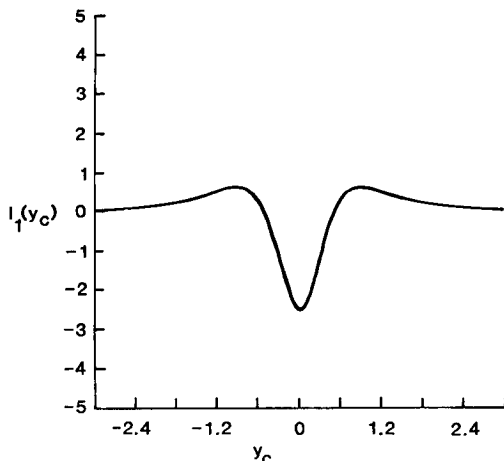


Fig. 4 Integral $I_1(y_c)$ for $\epsilon = 0.34$.

Plots of these expressions, again for the case $\epsilon = 0.34$, are shown over the range $-3 \leq y_c \leq 3$ in Figs. 4 and 5. Figures 6 and 7 also present numerically obtained derivatives of these expressions that are necessary in the noise calculation.

Comparison With Experiment

The theoretical analysis will be compared with the experimental work of Kambe, Minota, and Ikushima.⁴ Details of the experimental configuration are shown in Fig. 8. The experiment was carried out in a cubic anechoic chamber of side 1.8 m. The microphones were able to move in an arc in the plane $y_3 = 0$ at a distance of approximately 62 cm from the cylinder axis. A vortex ring, of radius 4.7 mm, was generated by a shock tube of 6 mm diam whose exit was a distance D upstream of the centerline and a distance L below it. The vortex speed V_s and the cylinder radius b are variable. The experiment was run several times, and average acoustic time histories were obtained. From a knowledge of the vortex speed and radius, the vortex circulation Γ may be estimated from the relation⁵

$$V_s = \frac{\Gamma}{4\pi r_v} \left(\ln \frac{8r_v}{\delta} - \frac{1}{4} \right) \quad (7)$$

where δ is the core radius of the vortex. Kambe, Minota, and Ikushima⁷ indicate that $\delta/r_v = 0.15$. Unfortunately, Kambe, Minota, and Ikushima⁴ did not measure the actual path traversed by the vortex. They assumed that the vortex traveled at a constant speed V_s that was estimated from measurement, along the line $Y_1(t) = L$ determined by the distance of the centerline of the shock tube below that of the cylinder. For his case, taking the time origin as the time at which the vortex

passes the centerline of the cylinder, $y_c(t) = V_s t/L$ and $\epsilon = r_v/L$ are constants. Thus, introducing an angle ϕ (measured from the negative y_2 -axis) such that $x_1/x = \sin\phi$ and $x_2/x = -\cos\phi$, Eq. (4) reduces to

$$p\left(x, t + \frac{x}{a_0}\right) = \frac{\rho_0 \Gamma \epsilon b^2 V_s^2}{4\pi a_0 x L^2} \left[\left(\frac{dI_1}{dy_c} \right) \sin\phi + 2 \left(y_c \frac{dI_2}{dy_c} + I_2 \right) \cos\phi \right] \quad (8)$$

There are at least three interesting aspects to this equation. First, note that in its derivation it has been assumed that 1) the

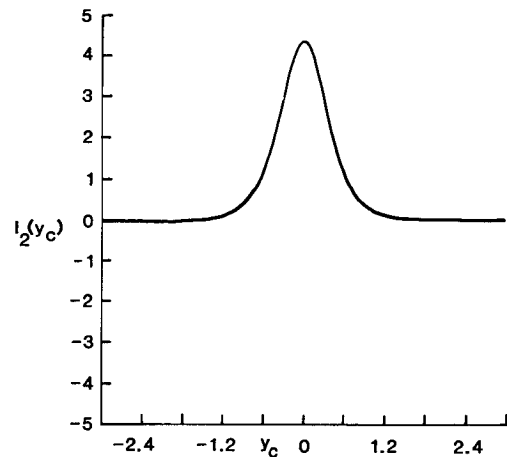


Fig. 5 Integral $I_2(y_c)$ for $\epsilon = 0.34$.

cylinder does not move, 2) the vortex path does not deviate from linear, 3) the vortex shape does not distort, and 4) the vortex speed is constant. Since a vortex in rectilinear, constant speed motion is silent, and fixed body is silent, what then generates the sound? The answer lies in the fluctuating force produced by the vortex on the cylinder.⁶ The negative of this force must, of course, act on the fluid, resulting in the production of a dipole sound field. Second, because this fluctuating force will vary in direction throughout the iteration, the directivity of the sound field will vary with time. This phenomenon will occur whenever a vortex passes a finite body (or vice versa), as in helicopter blade/vortex interaction. Finally, note the extreme sensitivity of this relation to the distance L of the vortex centerline below the cylinder centerline. Recalling that $\epsilon = r_v/L$, it can be seen from Eq. (8) that $p \sim L^{-3}$. Thus, if the distance L is increased by only 20%, the pressure is reduced to approximately half its previous value, whereas if the distance L is reduced by only 20%, the pressure is nearly doubled.

For the first experimental comparison, $L = 7.1$ mm and $b = 2.5$ mm. Thus, $\epsilon = 0.66$. Figure 9 displays the average acoustic pressure time histories at various angles ϕ [measured from the negative y_2 axis (see Fig. 8)]. Figure 10 is a similar plot of the theoretical results given by Eq. (8). The time axis for the theoretical results is source time t rather than observation time $t + x/a_0$. It proved impossible to equate the theoretical and experimental time origins. Some unexplained time shift is apparently present in the recorded data, as time calculated on the basis of the stated vortex convection velocity and nozzle distance D (see Fig. 8) does not agree with the experimental time axis. Note, however, the reasonable agree-

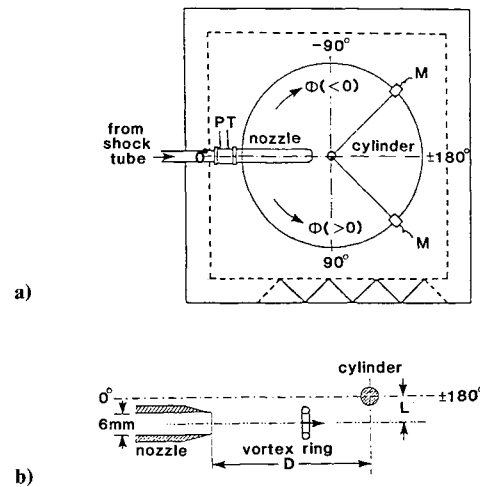


Fig. 8 Details of experimental configuration: a) anechoic chamber (M = microphone, PT = pressure transducer); b) arrangement of nozzle and cylinder.

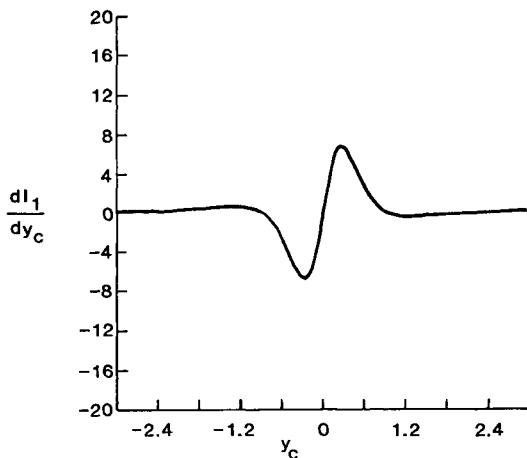


Fig. 6 Derivative dI_1/dy_c for $\epsilon = 0.34$.

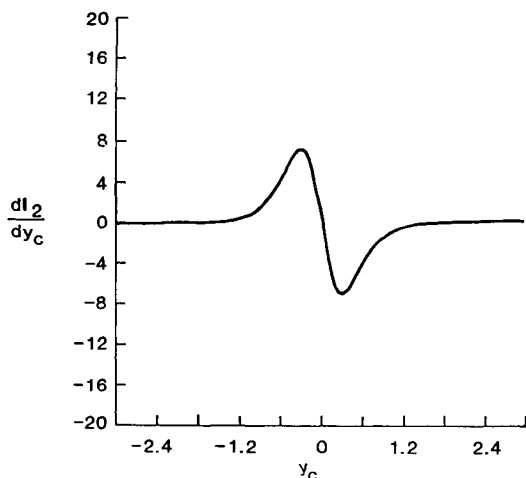


Fig. 7 Derivative dI_2/dy_c for $\epsilon = 0.34$.

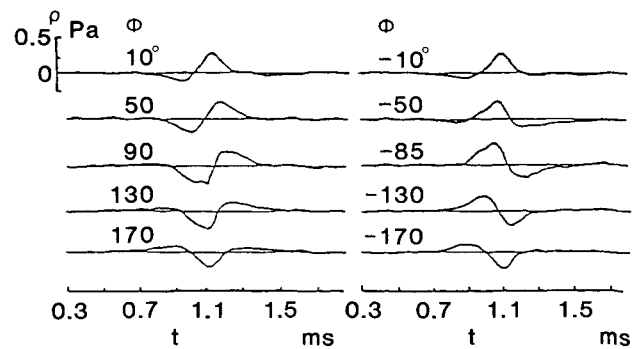


Fig. 9 Average sound pressure profiles of sound wave emitted by a vortex ring passing by the cylinder.

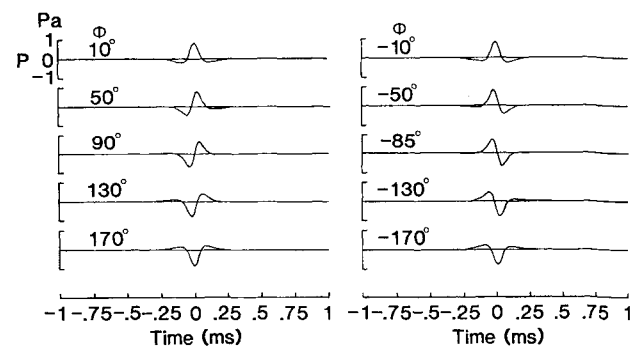


Fig. 10 Theoretical acoustic pressure time histories.

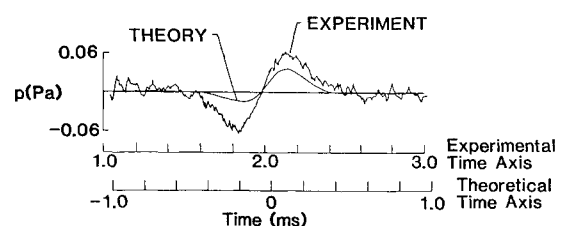


Fig. 11 Comparison of theoretical and experimental acoustic pressure time histories.

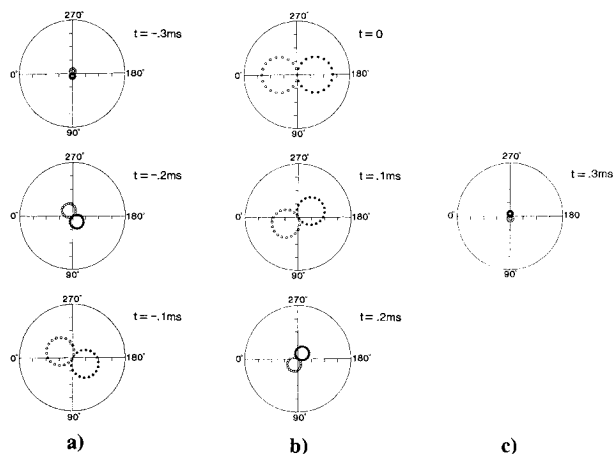


Fig. 12 Acoustic directivity as a function of time.

ment both in shape and magnitude (on a Pascal basis) of these acoustic time histories, although the theory overpredicts the peak values by a factor of approximately two. This overprediction can be understood by noting that this particular geometry (i.e., $b + r_v > L$) would produce a collision between the vortex and the cylinder. In reality, the vortex will avoid such a collision by ducking below the cylinder, thus increasing L . An increase in L by 20% (only 1.4 mm due to the small scale of the experiment) would account for the observed discrepancy.

A more precise comparison, which avoids the collision problem, can be obtained with the data published by Kambe.⁶ Here, L is increased to 13.2 mm, $V_s = 28$ m/s, and $b = 4.5$ mm. Thus, $b + r_v < L$ and $\epsilon = 0.36$. Figure 11 presents a comparison of the theoretical and experimental acoustic time histories at $\phi = 70$ deg. The time axes are matched by causing the zero crossings to coincide. Note that, in this case, the theory tends to underpredict the magnitude of the data, although the temporal extent is in good agreement. This comparison is not as good, however, as that published by Kambe⁶ using his less exact theory, although a small decrease in L could make it so. Whereas it can be shown that the extrema of Kambe's approximation are always smaller than those of the exact result, Kambe, Minota, and Ikushima do note in a previously published work⁷ that "a correction to the measured L is made," although this correction is unexplained. The required correction, on the order of 1 mm, is probably within the experimental error and suggests that their experiment should be repeated at a larger scale, where such high precision would not be required.

A further interesting aspect of this ring vortex/cylinder interaction is the directivity of the resulting noise generation. Figure 12 is a montage of polar plots of the acoustic pressure $p(x, \phi, t)$ vs ϕ at various times. Here, $x = 626$ mm, $V_s = 27$ m/s, $L = 13.5$ mm, $b = 4.5$ mm, and $\epsilon = 0.35$. The scale is linear, and the outer circle corresponds to a magnitude of 0.8 pascals. The

open theoretical points are positive pressure values, the closed points are negative values. The sound radiation can be seen to be dipole in nature, with the dipole axis rotating throughout the interaction. These results may be compared with the experimental data of Kambe,⁶ Fig. 7. The results are qualitatively similar except at $t = 0$ (vortex directly below cylinder), where Kambe's results show the dipole axis to be inclined rather than horizontal. Intuitively, the reason for the inclination of Kambe's result is not apparent.

Conclusions

This paper has re-examined the problem of sound radiation by the interaction of a ring vortex with a circular cylinder, which was previously analyzed by Minota and Kambe. The present analysis extends Minota and Kambe's work by allowing the vortex path to be arbitrary and by exact integration of the integrals arising in the noise calculation. On the basis of this work, several conclusions may be drawn:

- 1) Noise will be produced by such an interaction even in the absence of any acceleration of the vortex. If the vortex accelerates, or its path deviates from linear, additional sound may be generated.
- 2) The amplitude of the sound radiation is sensitively dependent upon the distance at which the vortex passes by the cylinder.
- 3) The resulting dipole sound field rotates throughout the interaction.
- 4) The clean experiment of Kambe, Minota, and Ikushima should be repeated at a larger scale, where experimental accuracy would not so critically influence the comparison between theory and experiment, and the precise path of the vortex should be measured.

References

- ¹Minota, T. and Kambe, T., "Acoustic Waves Emitted by a Vortex Ring Passing Near a Circular Cylinder," *Journal of Sound and Vibration*, Vol. 119, No. 3, Dec. 1987, pp. 509-528.
- ²Obermeier, F., "The Influence of Solid Bodies on Low Mach Number Vortex Sound," *Journal of Sound and Vibration*, Vol. 72, No. 1, Sept. 1980, pp. 39-49.
- ³Howe, M.S., "Contributions to the Theory of Aerodynamic Sound with Application to Excess Jet Noise and the Theory of the Flute," *Journal of Fluid Mechanics*, Vol. 71, Pt. 4, Oct. 1975, pp. 625-673.
- ⁴Kambe, T., Minota, T., and Ikushima, Y., "Aerodynamic Sound Emission by a Vortex Ring in the Vicinity of Solid Bodies," *Proceedings of the 10th International Congress on Nonlinear Acoustics*, North Holland, Amsterdam, 1984, pp. 239-244.
- ⁵Kambe, T., and Minota, T., "Acoustic Wave Radiated by Head-on Collision of Two Vortex Rings," *Proceedings of the Royal Society of London*, Ser. A, Vol. 386, 1983, pp. 277-308.
- ⁶Kambe, T., "Acoustic Emissions by Vortex Motions," *Journal of Fluid Mechanics*, Vol. 173, Dec. 1986, pp. 643-666.
- ⁷Kambe, T., Minota, T., and Ikushima, Y., *Acoustic Waves Emitted by Vortex-Body Interaction, Aero- and Hydro-Acoustics*, edited by G. Comte-Bellot and J.E. Ffowcs Williams, Springer-Verlag, Berlin, 1986, pp. 21-28.